Broadband electron spin resonance from 500 MHz to 40 GHz using superconducting coplanar waveguides

C. Clauss,[1] D. Bothner,[2] D. Koelle,[2] R. Kleiner,[2] L. Bogani,[1] M. Scheffler,[1] and M. Dressel[1]

[1] *1. Physikalisches Institut, Universität Stuttgart, Pfaffenwaldring 57, D-70550 Stuttgart, Germany*

[2] *Physikalisches Institut and Center for Collective Quantum Phenomena in LISA$^+$, Universität Tübingen, Auf der Morgenstelle 14, D-72076 Tübingen, Germany*

(Dated: September 25, 2012)

We present non-conventional electron spin resonance (ESR) experiments using microfabricated superconducting waveguides. We show that a very broad frequency range, from 0.5 to 40 GHz, becomes accessible with a high frequency accuracy of less than 1 MHz at low temperatures down to 1.6 K and in fields up to 1.4 T. This allows an accurate inspection of the ESR absorption position in the frequency domain, in contrast to the more common observation in the field domain. We demonstrate the applicability of frequency-swept ESR on Cr^{3+} atoms in ruby as well as on organic radicals of the Nitronyl-nitroxide family (using the 2-(4'-methoxyphenyl)-4,4,5,5-tetra-methylimidazoline-1-oxyl-3-oxide, a.k.a. NitPhOMe). Measurements between 1.6 and 30 K reveal a small frequency shift of the ESR and a resonance broadening below the critical temperature, which we both attribute to a modification of the magnetic field configuration due to the appearance of shielding currents.

PACS numbers: 87.80.Lg, 76.30.Rn, 84.40.Az, 07.57.Pt

arXiv:1209.5061v1 [cond-mat.mes-hall] 23 Sep 2012

One of the main challenges in electron spin resonance (ESR) has always been to attain higher sensitivities. The main strategy to achieve this was to use resonant cavities with higher and higher fields and frequencies. As a result, most modern instrumentation can operate only at a single frequency or in an extremely narrow frequency range [1]. However, this can be a serious hindrance when a frequency-dependent effect is to be observed, as needed to probe a complete phase diagram of some material or to reliably assess the distance and orientation of spin labels. The latter problem, in particular, is increasing in importance in the domain of biological ESR, as it is fundamental to understand the structural conformation and dynamics of biological systems. Until now the main strategy to overcome such problems was to measure the response of the system at a few discrete and widely-spaced frequencies [2].

Another approach is to reduce the dimension of the ESR cavities to micrometer size while at the same time somewhat relaxing the resonance requirements [3–5]. In this way small sample quantities can be probed over a wider frequency range. Setups that offer the possibility to sweep both the magnetic field and the radiation frequency have so far mostly been realized in the high frequency region (quasi-optical, from 50 to several 100 GHz) [6–8], while lower frequencies have been inspected using a coupled antenna approach [9] or tuneable cavities [10].

In this letter we demonstrate a different approach which uses a microfabricated superconducting coplanar waveguide to generate the radio frequency (RF) field. The feasibility of such an approach was shown before by Schuster *et al.* focusing on high-cooperativity coupling of spin ensembles to superconducting cavities [11]. Related devices (striplines, microstrips) are also used to study ferromagnetic resonances of various materials [12–14]. We show that it is possible to probe both the frequency and field dependence of ESR lines in a very wide frequency range from 0.5 to 40 GHz. We demonstrate the applicability of the method on a ruby single crystal (Al_2O_3:Cr^{3+}, see Fig. 1(d)), as well as on a Nitronyl-nitroxide radical, 2-(4'-methoxyphenyl)-4,4,5,5-tetra-methylimidazoline-1-oxyl-3-oxide (NITPhOMe for short, see Fig. 1(c)), which is a very clean and isotropic $S = \frac{1}{2}$ system that is widely used as spin label for biological systems and as a building block for single chain magnets. The results show, that this technique is particularly suited to precisely determine the zero-field-splitting (D-values in the spin Hamiltonian) and the weight of higher order anisotropy terms of multilevel spin systems (which play an important role in e.g. rare earth coordination compounds).

Figure 1(a) shows a sketch of a coplanar waveguide. The signal carrying center conductor line is flanked by two ground planes which act as the outer conductor/shielding. The devices are fabricated by sputtering a 150 nm thick niobium film on top of a 330 µm thick r-cut sapphire substrate and structuring the film with UV lithography (center conductor width: 60 µm, center-ground plane separation: 25 µm). The Nb films have a superconducting critical temperature $T_c \approx 9$ K and a residual resistance ratio of $R_{300\ \mathrm{K}}/R_{10\ \mathrm{K}} \approx 6$. The resulting chip ($7 \times 4\mathrm{mm}^2$) is mounted into a gold-plated brass box and contacted with silver paste to sub-miniature A (SMA) stripline connectors (center conductor) and the box (ground planes). In case of the NITPhOMe sample, a small amount (< 0.5 mg) of crystallites was dissolved in isopropyl and dropwise transferred to the waveguide. After evaporation of the solvent, the radicals were permanently attached to the waveguide structure (blue area in Fig. 1(g)). For the ruby sample, a polished

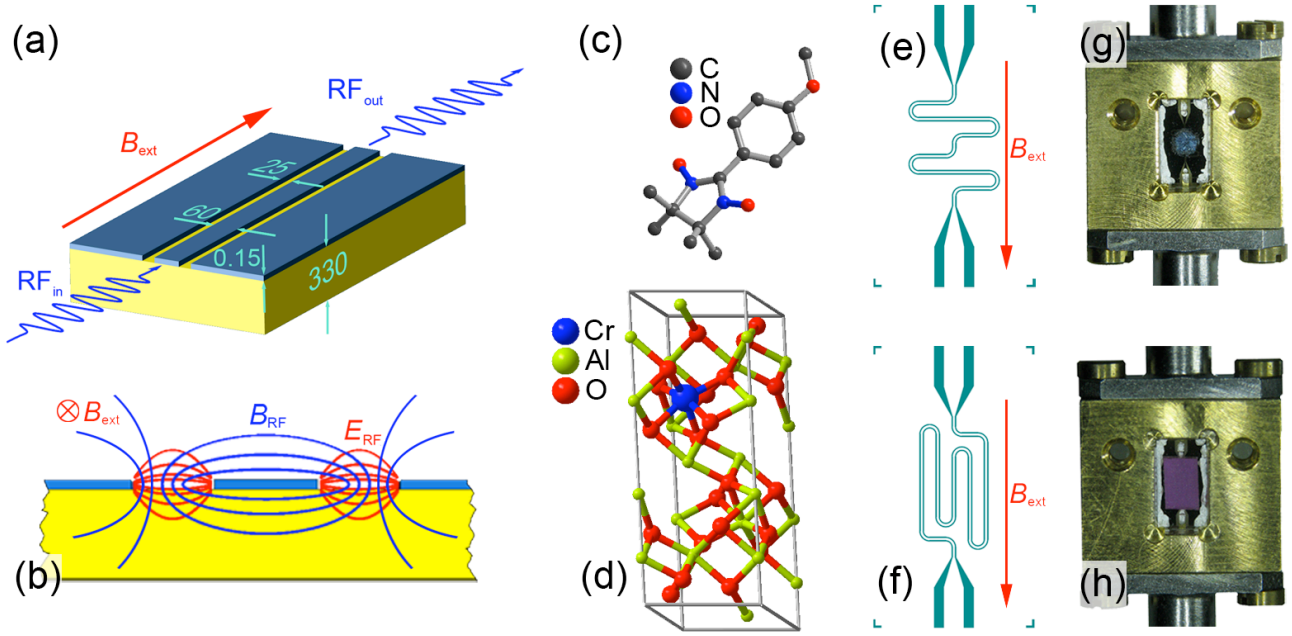

FIG. 1: (color online) (a) Schematic layout of a coplanar waveguide and its orientation with respect to the external magnetic field in this experiment. (b) Schematic cross-sectional view of the planar structure and sketched electric and magnetic field distribution of the microwave field. (c) Structure of NITPhOMe. The spin density is maximized at the N-O parts. (d) Unit cell of ruby. (e) and (f) Layout of the waveguide geometry used for the NITPhOMe and ruby experiments, respectively. (g) and (h) Photos of the mounted waveguides and samples.

brick-shaped crystal ($2.5 \times 4 \times 1$ mm^3) was put directly on the chip and fixed with vacuum grease (see Fig. 1(h)). This assembly is then cooled in a magnet cryostat. Unless noted otherwise, all data shown in this letter were acquired at 1.6 K.

For all the presented experiments the external magnetic field is oriented parallel to the film (see Figure 1(a))[19]. Note that only for an orientation as shown in Figure 1(a) the magnetic field component of the microwave signal (B_{RF}) is perpendicular to the static external field (B_{ext}) and thus fulfills the requirement to induce spin flips between the Zeeman-split levels (see also Figure 1(b)). For the designs used, the waveguide meanders over the chip and only parts of it are oriented in the correct way (see Fig. 1(e),(f)). While for the NITPhOMe sample this portion is only 120 µm, it is much longer (8 mm) for the measurements on the ruby sample.

In both cases a continuous wave microwave signal (input power $P_{\mathrm{in}} = -20$ dBm) is fed via coaxial cables to the cooled waveguide with the sample, and the transmitted power is recorded with a power meter (NITPhOMe) or with a vector network analyzer (ruby). For the frequency-swept spectra the transmitted power is recorded as a function of frequency at a static external field B_{ext}. A typical transmission spectrum is shown in Figure 2(a). The transmission decreases with increasing frequency due to the frequency-dependent attenuation of the coaxial cables and the coplanar line.

To identify the signal arising from spin transitions in the sample, the spectra taken at finite external magnetic field B_{ext} have to be normalized. The simplest approach is using the zero field spectrum for normalization of all other spectra (see Figure 2(b)). This however turned out to be problematic, since in addition to a change in the overall transmission through the superconducting waveguide due to losses resulting from movement of vortices [15, 16] there are field dependent features appearing around certain frequencies. These features appear in the normalized spectra and can obscure the ESR signal (see upper curve in Figure 2(b)). These features (around 5 GHz) are supposed to be box modes and standing waves on the waveguide between the connectors or on the ground planes. They change in magnetic field due to the change of the high frequency transport properties of the superconducting film. These spurious modes change slightly for different waveguides or sample holder boxes. It is therefore not trivial to compensate for them.

However, since both the increase of attenuation of the superconducting waveguide as well as the variation of box mode absorption evolve only slowly with magnetic field, one can use a spectrum taken at a slightly different field for normalization. Here we found that spectra taken at 10 mT higher fields result in a straight baseline at unity and a rather good suppression of the evolving parasitic features (see lower line in Figure 2(b)). A selection of spectra normalized in this manner is shown Figure 2(c) for fields from 20 to 340 mT in 20 mT steps for a frequency range from 100 MHz to 10 GHz (in fact the absorption for every 10 mT can be seen

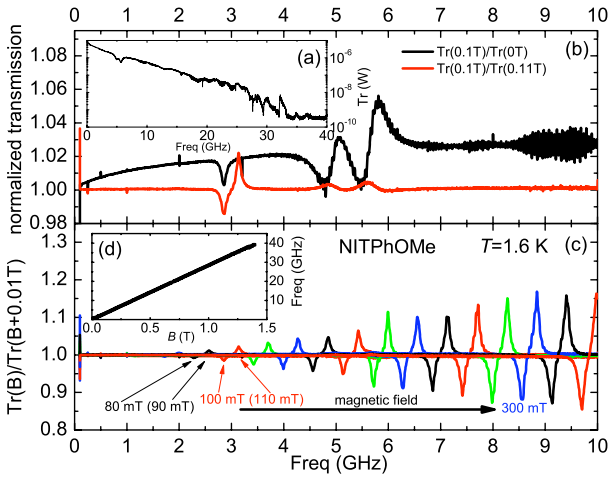

FIG. 2: (color online) (a) Broadband transmission spectra at zero field at 1.6 K. (b) Example for the data analysis for the field-swept spectra. Black: Spectrum at 0.1 T normalized to zero field spectrum. Red/Gray: Spectrum at 0.1 T normalized to spectrum at 0.11 T (c) frequency-swept spectra for fields ranging from 20 to 340 mT at 20 mT steps (very low field absorptions not visible at this scale). (d) Position of the absorption peak minimum vs. magnetic field for all measured spectra.

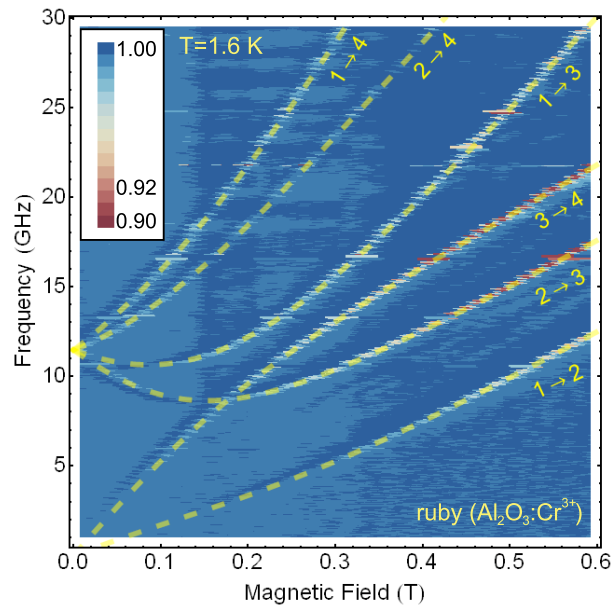

FIG. 3: (color online) Normalized frequency-swept ESR spectra for ruby. Lighter and red areas show the ESR absorption positions and dashed lines show a fit to the transitions between the eigenfunctions of the Cr^{3+} spin Hamiltonian. The different spin states are labeled as 1: $m_s = -\frac{3}{2}$, 2: $m_s = -\frac{1}{2}$, 3: $m_s = +\frac{1}{2}$ and 4: $m_s = +\frac{3}{2}$

since the peaks above unity belong to the spectra used for normalization). The signal intensity increases with increasing external field due to the increasing thermal population difference of the Zeeman split energy levels.

As can be seen from Figure 2(a) the transmission steadily decreases with increasing frequency up to about 33 GHz. Due to the connectors, which are not recommended for frequencies above 25 GHz, the measured transmitted power for higher frequencies is close to the detection limit of the power meter and the spectra get very noisy. Despite the high noise level, the absorption peaks can still be identified and their position is plotted vs. the external magnetic field in Figure 2(d). From the slope of that curve ($h\nu = g\mu_B B_{\text{ext}}$) a g-value of $g = 2.019 \pm 0.001$ was extracted.

We also performed frequency-swept ESR on a ruby sample of unknown crystallographic orientation for a frequency range from 1 to 30 GHz and fields up to 0.6 T in 7.5 mT steps. The resulting normalized spectra ($\text{Tr}(B/\text{Tr}(B + 0.015\ \text{T}))$) are shown as a color map plot in Fig. 3 for a range from 0.9 to 1.0 (to not show the peaks of the reference spectra). All possible transitions between the four states of the zero-field-split quartet can be seen over almost the complete magnetic field and frequency range. The lighter and red regions denote the positions of ESR absorptions and solid lines are transitions calculated from the Cr^{3+} spin Hamiltonian for an orientation of B_{ext} at 78° to the c-axis of the crystal [17, 18]. Since every frequency-swept spectrum can be used to fit unknown parameters of the spin Hamiltonian, this method could be used to determine the weight of higher order anisotropy terms for more complex (low symmetry) materials.

In addition to the frequency-swept spectra, we also performed magnetic-field-swept ESR. Several selected spectra are shown in Figure 4. Here, we record the transmitted power at fixed frequencies as a function of applied external field. The off-resonance transmission decreases with increasing field/frequency due to the frequency-dependent attenuation mentioned above. Figure 4 (b) shows a set of field-swept spectra taken at the upper edge of the accessible frequency range, demonstrating that ESR can be detected for frequencies as high as 40 GHz.

Although the high frequency losses of the waveguide are minimized when working at temperatures below T_c, we were also able to detect the ESR signal of NITPhOMe at temperatures well above T_c. The temperature dependence of a selection of frequency-swept spectra for $B_{\text{ext}} = 1$ T (spectra were normalized with those at $B_{\text{ext}} = 1.05$ T) is shown in Fig. 5. Upon cooling down from 30 K, we observe an increase of the peak amplitude due to the increase of imbalance of thermal occupation. Reaching the critical temperature of the Nb film (for these fields at around 5 K) and cooling further, two effects can be observed. (1) While crossing the transition temperature, the baseline deviates from unity due to different transport properties of the metallic film for the spectra recorded at $B_{\text{ext}} = 1$ T compared to the reference spectrum recorded at $B_{\text{ext}} = 1.05$ T. (2) Below T_c the peak frequency of the ESR signal shifts to

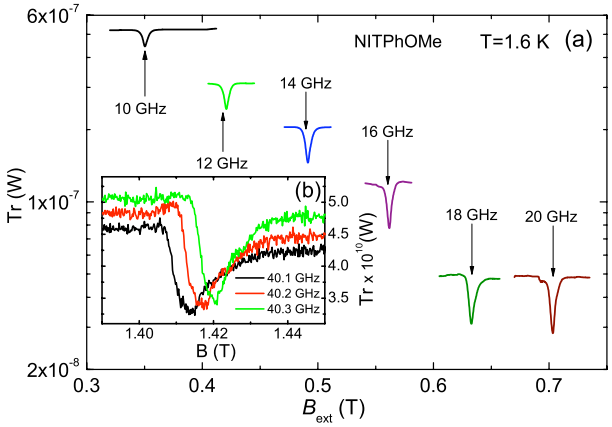

FIG. 4: (color online) (a) Field-swept spectra for various frequencies. The absolute value of the transmitted power off-resonance is predominantly determined by the frequency-dependent damping of the coaxial lines. Inset (b): Field swept spectra around 40 GHz.

slightly higher frequencies and the absorption dip gets broadened. We attribute this effect to a modification of the local magnetic field by shielding currents in the superconductor. Directly at the surface of the Nb planes – and hence also in the gaps between center conductor and ground planes – the magnetic field is enhanced as compared to the normal conducting state, which shifts the Zeeman splitting of spins sitting directly at the surface to higher values. With increasing distance from the Nb surface the field values approach B_{ext} and due to this field inhomogeneity we not only get a shift but also a broadening of splitting energies and of the ESR absorption dip. As also the amplitude of B_{RF} and hence the amplitude of the ESR depends on the position on the

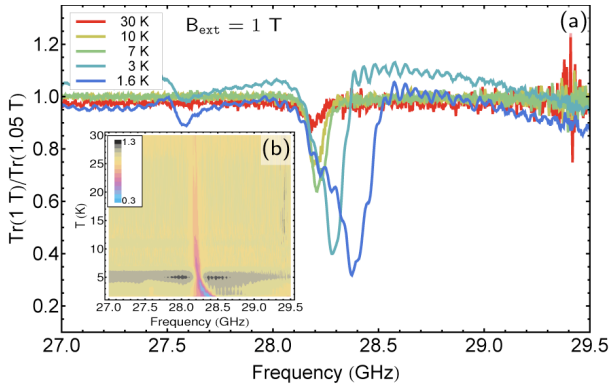

FIG. 5: (color online) (a) frequency-swept spectra for several selected temperatures. The absorption is already visible for temperatures above T_c. Upon cooling through the superconducting transition, the absorption peak frequency shifts to higher frequencies. (b) All measured spectra shown in a contour map. The transition into the superconducting state around 5 K as well as the shift of the ESR absorption for temperatures below T_c is clearly visible.

chip and decreases with distance from the surface, the exact overall situation in the superconducting state is rather complicated. However, the effect of the modified field profile in our experiments is rather small (about 1%) but nevertheless has to be considered when it comes to precise determination of ESR frequencies with superconducting waveguides.

In conclusion, we have shown that microfabricated superconducting structures can be used for broadband ESR spectroscopy over a wide range of frequencies and magnetic fields. The temperature-dependent results show a good performance of our system even above the critical temperature and suggest the use of non-superconducting materials to probe ESR over an even wider range of temperatures. Due to the compact design, the device could easily be used down to 1.6 K and provides the possibility to perform ESR experiments in a dilution refrigerator, reaching the mK regime. We demonstrated the novel approach for two very different preparation methods, from liquid to solid-state samples, showing a wide range of applicability. A complete frequency-field characterization is now possible (see Fig. 3) and the technique thus offers the possibility to characterize a variety of materials with high precision. In particular it is suited to determine the orientation of anisotropy axes, large zero-field-splittings and will provide access to higher-order anisotropy terms of high-spin systems. It is thus expected to be particularly useful for the characterization of molecular materials and rare-earth based magnets. The combination of a wide frequency and field range will also be useful for the spectroscopic determination of level mixing (avoided level crossings), which are expected in many magnetic molecular clusters. Eventually it is important to understand that the technique can readily be exported to the pulsed domain. The demonstrated applicability to Nitronyl-nitroxide spin-labels shows that the technique can be applied to provide the accurate, frequency-domain information needed for the structural characterization of biological structures.

This work was supported by the Deutsche Forschungsgemeinschaft, including SFB/TRR 21 and SPP1601 and the Humboldt Stiftung via the Sofja Kovalevskaja prize. DB gratefully acknowledges support by Evangelisches Studienwerk e.V. Villigst.

[1] Ch. P. Poole, Jr., *Electron Spin Resonance: A Comprehensive Treatise on Experimental Techniques*, 2nd ed., (Dover Publications Inc. 1997).

[2] S. K. Misra, *Multifrequency Electron Paramagnetic Resonance*, (Wiley-VCH 2011).

[3] R. Narkowicz, D. Suter, and R. Stonies, J. Magn. Reson. **175**, 275 (2005).

[4] R. Narkowicz, D. Suter, and I. Niemeyer, Rev. Sci. Instrum. **79**, 084702 (2008).

[5] H. Malissa, D. I. Schuster, A. M. Tyryshkin, A. A. Houck, and S. A. Lyon, arXiv:1202.6305v1, (2012).

[6] E. J. Reijerse, Appl Magn Reson **37**, 795 (2010).

[7] D. Gatteschi, Lecture Notes in Physics **595**, 454 (2002).

[8] J. van Slageren, S. Vontragool, B. Gorshunov, A. A. Mukhin, N. Karl, J. Krzystek, J. Telser, A. Mller, C. Sangregorio, D. Gatteschi, and M. Dressel, Phys. Chem. Chem. Phys. **5**, 3837 (2003).

[9] Z. H. Jang, B. J. Suh, M. Corti, L. Cattaneo, D. Hajny, F. Borsa, and M. Luban, Rev. Sci. Instrum. **79**, 046101 (2008).

[10] C. Schlegel, M. Dressel, and J. van Slageren, Rev. Sci. Instrum. **81**, 093901 (2010).

[11] D. I. Schuster, A. P. Sears, E. Ginossar, L. DiCarlo, L. Frunzio, J. J. L. Morton, H. Wu, G. A. D. Briggs, B. B. Buckley, D. D. Awschalom, and R. J. Schoelkopf, Phys. Rev. Lett. **105**, 140501 (2010).

[12] G. Goglio, S. Pignard, A. Radulescu, L. Piraux, I. Huynen, D. Vanhoenacker, and A. Vander Vorst, Appl. Phys. Lett. **75**, 1769 (1999).

[13] F. Giesen, J. Podbielski, T. Korn, M. Steiner, A. van Staa, and D. Grundler, Appl. Phys. Lett. **86**, 112510 (2005).

[14] Yan Liu, Linfeng Chen, C. Y. Tan, H. J. Liu, and C. K. Ong, Rev. Sci. Instrum. **76**, 063911 (2005).

[15] C. Song, T. W. Heitmann, M. P. DeFeo, K. Yu, R. McDermott, M. Neeley, J. M. Martinis, and B. L. T. Plourde, Phys. Rev. B **79**, 174512 (2009).

[16] D. Bothner, C. Clauss, E. Koroknay, M. Kemmler, T. Gaber, M. Jetter, M. Scheffler, P. Michler, M. Dressel, D. Koelle, and R. Kleiner, Appl. Phys. Lett. **100**, 012601 (2012).

[17] J. Weber, Rev. Mod. Phys. **31**, 681 (1959).

[18] E. O. Schulz-DuBois, BellSyst. Tech. J. **38**, 271 (1959).

[19] The experimental insert is designed for a film orientation parallel to the magnetic field. At this moment, we cannot quantify the misalignment of the field, but we estimate a tilting out of plane of less than 2°.